

Electronic Supplementary Information

Tuning electrical and magnetic properties in multifunctional composite materials based on PEDOT:DBS conducting polymer and magnetite nanoparticles

Matías Lanús Mendez Elizalde,^a Carlos Acha,^b M. Sergio Moreno,^c P. Soledad Antonel^{*a}

a Instituto de Química Física de Materiales, Ambiente y Energía (INQUIMAE) and Departamento de Química Inorgánica, Analítica y Química Física, Facultad de Ciencias Exactas, Ciudad Universitaria, Pabellón 2, C1428EHA, Buenos Aires, Argentina.

b Laboratorio de Bajas Temperaturas, Departamento de Física, Facultad de Ciencias Exactas y Naturales, Universidad de Buenos Aires and IFIBA (UBA-CONICET), Ciudad Universitaria, Pabellón I, C1428EHA, Buenos Aires, Argentina.

c Instituto de Nanociencia y Nanotecnología, Centro Atómico Bariloche, San Carlos de Bariloche, Rio Negro, Argentina.

Particle size and composites morphology

From TEM and SEM images (Figures 1 and 2) of all the synthesized materials, the MNP diameters were measured with the aid of ImageJ software. The resulting histograms and log-normal distributions are presented in Figure S1.

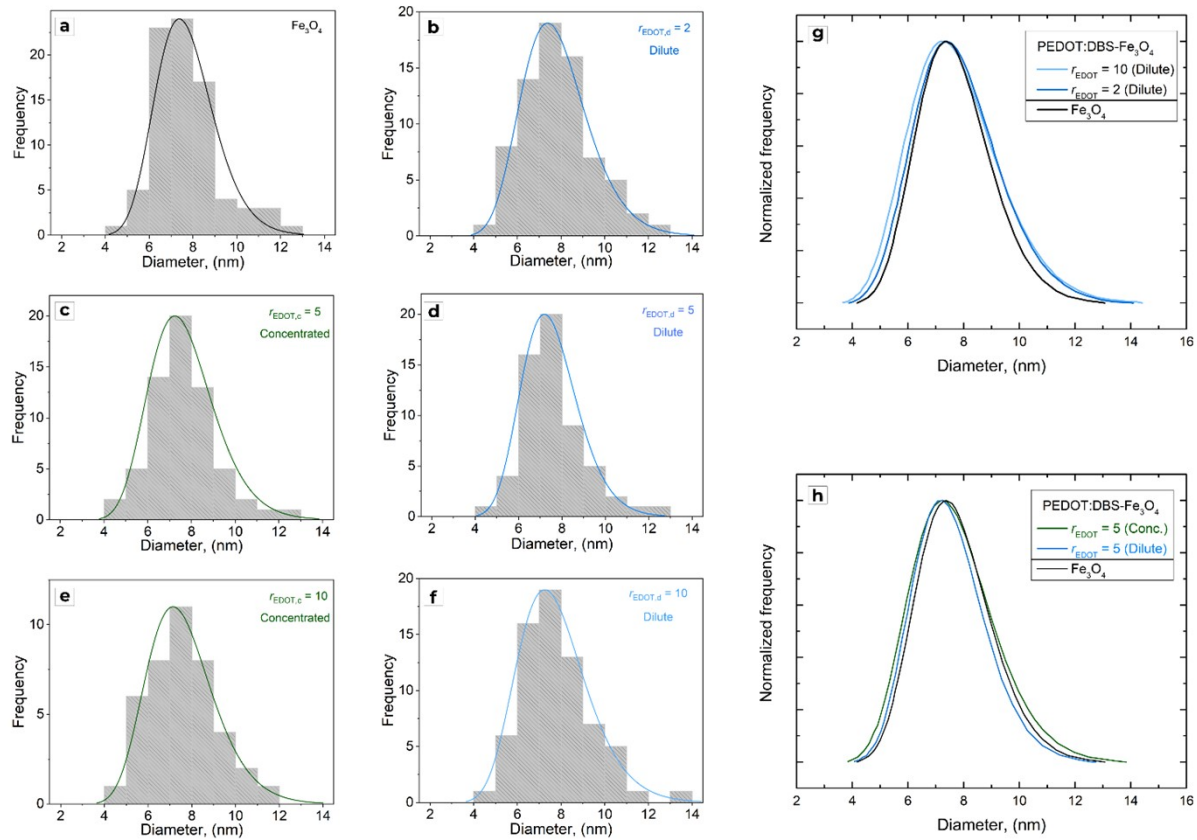


Figure S1. Particle diameters distribution for (a) Fe_3O_4 MNP and PEDOT:DBS- Fe_3O_4 composites with: (b) $r_{\text{EDOT},d} = 2$; (c) $r_{\text{EDOT},c} = 5$; (d) $r_{\text{EDOT},d} = 5$; (e) $r_{\text{EDOT},c} = 10$; (f) $r_{\text{EDOT},d} = 10$. Superimposed curves: (g) and (h).

The mean particle diameter, D_p , of bare Fe_3O_4 MNP was found to be 7.6 nm, with a standard deviation, SD, of 1.2 nm. Also, the mode was determined, obtaining a value of 7.4 nm. Regarding PEDOT:DBS- Fe_3O_4 composites, similar values for mean D_p , SD and modes were obtained for the MNP in the materials. Moreover, all the D_p distributions of the composites are almost superimposed with the one observed for bare Fe_3O_4 MNP (Figure S1 (g) and (h)). The statistical values of each distribution are presented in Table S1.

Table S1. Statistical parameters (SD: standard deviation; FWHM: full width at half maximum; GSD: geometrical standard deviation) obtained for the nanoparticle diameters in all the synthesized materials. Also, the corresponding PDI (diameter polydispersity index) are informed. The analysis was performed by measuring 60-75 MNP diameters in the corresponding electron microscopy images.

Material	D_p (nm)					GSD
	Mean	Mode	SD	FWHM	PDI	
$r_{\text{EDOT},d} = 2$	7.8	7.4	1.5	3.5	0.037	1.2
$r_{\text{EDOT},d} = 5$	7.5	7.3	1.4	3.0	0.035	
$r_{\text{EDOT},d} = 10$	7.7	7.3	1.7	3.7	0.049	
$r_{\text{EDOT},c} = 5$	7.7	7.3	1.5	3.4	0.038	
Fe_3O_4	7.7	7.4	1.2	3.0	0.025	

From these results, it is deduced that the maximum shift of the diameters distribution is 0.3 nm, whereas the maximum broadening results in 0.7 nm. Considering, also, that the same geometrical standard deviation (GSD) of 1.2 was obtained in all cases, these results indicate that the MNP size remains unchanged after the composite formation.

Furthermore, the diameter polydispersity index (PDI) was calculated in each case from the electronic microscopy images, following Lavorato et al¹:

$$PDI = \left(\frac{SD_{D_p}}{Mean_{D_p}} \right)^2 \quad (E1)$$

and the obtained PDI values are also included in Table S1. It is clear that, although there is a small increase in the calculated values as both r_{EDOT} and the concentration of reactants increase, MNP size dispersion is considerably low in comparison with that obtained with other MNP synthesis methods¹. This is probably due to the higher synthesis temperature and longer digestion time employed in our work. These results indicate that Fe₃O₄ MNP embedded in the PEDOT matrix conserve their mean size.

Also, a MNP shape analysis was performed, based in the HR-TEM images of PEDOT:DBS-Fe₃O₄ composite obtained with $r_{EDOT,d} = 2$. The 2D area of the MNP, as observed in the HR-TEM images, were measured with the aid of ImageJ software, and plotted against the equivalent round area, A_{eq} , defined as $A_{eq} = \pi(D_p/2)^2$, as presented in Fig. S2a. Expected areas for spherical and cubic shapes were also plotted against A_{eq} for comparison (dotted lines in Fig. S2a). The deviation from the identity indicates that MNP are not spherical shaped, in fact, the MNP have cubic-like shapes. Fig. S2b present some of the MNP areas as found for the PEDOT:DBS-Fe₃O₄ composite prepared with $r_{EDOT,d} = 2$.

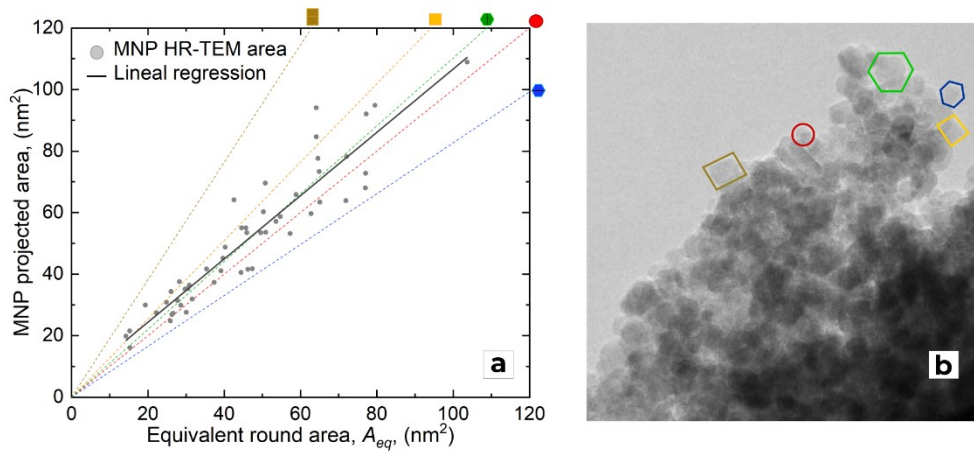


Figure S2. (a) MNP 2D areas (as observed in HR-TEM images, grey dots) vs. A_{eq} . Dotted lines: expected areas for spherical and cubic shapes sharing the same section vs. A_{eq} . (b) HR-TEM image of PEDOT:DBS-Fe₃O₄ composite prepared with $r_{EDOT,d} = 2$. Color shapes denote the corresponding areas of spherical (red) and cubic (blue, green, yellow, and brown) geometries.

Similar MNP shapes were found in PEDOT:DBS-Fe₃O₄ composites, for all the r_{EDOT} and feed concentrations explored in this work, indicating that the shape of Fe₃O₄ nanoparticles is not affected by synthetic conditions employed for the polymerization of EDOT. This observation is in agreement with previous works based on composites of ferrite MNP and conducting polymers synthesized under similar procedures^{2,3}.

Magnetization behavior and magnetic interactions

In the following, we described the $M(H,T)$ curves (ZFC and FC) using a formalism based on non-interacting MNP (Stoner-Wolfarth), where L is the Langevin function and the effects of the size dispersion were associated to a dispersion of blocking temperatures (T_B) following a lognormal distribution, as indicated on the following equations⁴:

$$\frac{M_{ZFC}(H,T)}{M_s(T)} = \frac{1}{\langle T_B \rangle} \left[\int_0^T L\left(\frac{\mu_0 M_s H}{K T}\right) T_B f(T_B, T_{B0}, s) dT_B + \frac{\mu_0 M_s H}{3 K} \int_T^\infty T_B f(T_B, T_{B0}, s) dT_B \right]$$

$$\cong \frac{\mu_0 M_s H}{3 K \langle T_B \rangle} \left[\frac{25}{T} \int_0^T T_B^2 f(T_B, T_{B0}, s) dT_B + \int_T^\infty T_B f(T_B, T_{B0}, s) dT_B \right], \quad (E2)$$

$$\frac{M_{FC}(H, T)}{M_s(T)} = \frac{1}{\langle T_B \rangle} \left[\int_0^T L\left(\frac{\mu_0 M_s H 25 T_B}{K T}\right) T_B f(T_B, T_{B0}, s) dT_B + \int_T^\infty L\left(\frac{\mu_0 M_s H 25}{K}\right) T_B f(T_B, T_{B0}, s) dT_B \right]$$

$$\cong \frac{25 \mu_0 M_s H}{3 K \langle T_B \rangle} \left[\frac{1}{T} \int_0^T T_B^2 f(T_B, T_{B0}, s) dT_B + \int_T^\infty T_B f(T_B, T_{B0}, s) dT_B \right], \quad (E3)$$

where $f(T_B, T_{B0}, s)$ is the lognormal distribution function, with T_{B0} and s being the median blocking temperature value and the shape parameter of the distribution, respectively. For the approximation we have considered that $L(x)=x/3$ for $x \rightarrow 0$. $\langle T_B \rangle$ is the mean blocking temperature [$\langle T_B \rangle = T_{B0} \exp(s^2/2)$], k_B the Boltzmann constant, M_s the saturation magnetization and K the magnetic anisotropy constant. T_{B0} , s , M_s and K were considered as fitting parameters. The obtained values are shown in Table S1. The mean diameter of the MNP ($\langle d \rangle$) can be derived from its volume relation,

$$\langle v \rangle = \frac{25}{K} k_B \langle T_B \rangle = \frac{\pi}{6} \langle d \rangle^3 \quad (\text{assuming a spherical shape for the MNP}).$$

Table S2. Fitting parameters: median blocking temperature T_{B0} , shape parameter s (standard deviation of the log of the distribution), anisotropic constant K and saturation magnetization M_s . Calculated values of median and mean MNP diameter, d and $\langle d \rangle$, respectively, and mean blocking temperature $\langle T_B \rangle$, are also presented. Highlighted in green: good fit for ZFC and poor for FC. Highlighted in blue: good fit for ZFC and poor for FC.

Parameters	PEDOT: DBS-Fe ₃ O ₄		
	$r_{\text{EDOT},d} = 5$		$r_{\text{EDOT},c} = 5$
Fit for ZFC	Good	Bad	Good
Fit for FC	Bad	Good	Bad
T_{B0} , (K)	40	160	38.5
s	0.9	0.88	0.86
K , (J/m ³)	12000	56400	13000
M_s , (A/m)	95800	129500	88100
d , (nm)	13	12.3	12.5
$\langle d \rangle$, (nm)	14.9	14	14.1
$\langle T_B \rangle$, (K)	60	235	55.8

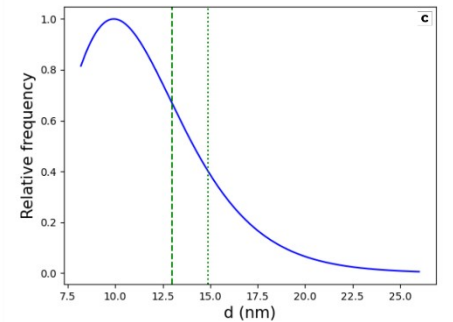
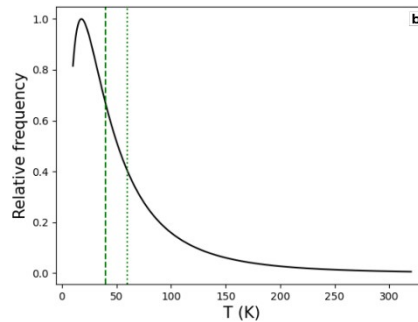
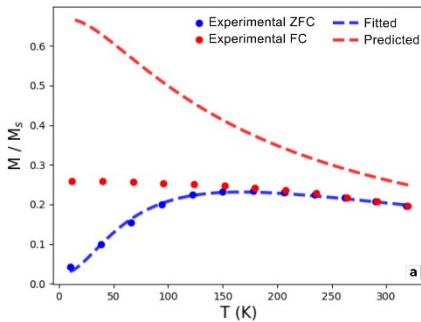


Figure S3. (a) ZFC and FC curves of PEDOT:DBS-Fe₃O₄ with $r_{EDOT,d} = 5$. Experimental data are represented with dots, and fitting data with short lines. (b) T_B distribution obtained from fitting for the PEDOT:DBS-Fe₃O₄ material prepared with $r_{EDOT,d} = 5$. (c) Diameter distribution obtained from fitting for PEDOT:DBS-Fe₃O₄ material prepared with $r_{EDOT,d} = 5$. Median and mean values are indicated by dashed and dotted lines, respectively.

In Fig. S3a the ZFC was initially fitted and then the FC curve was predicted with the obtained parameters. As it can be seen, the parameters that minimize residues in the ZFC fitting fail to reproduce the FC flat experimental response of the composite. This is evident by comparing the residual values for each fitting in Table S1. Moreover, the experimental FC curve shape seems flatter than the predicted one, as discussed in the manuscript. Fig. S3b and S3c show the T_B distribution and the diameter distributions as obtained from the fitted parameters following Micha et. al.⁵, Mamiya et al.⁶ and Bruvera et al.⁷

In Fig. S4a the FC was initially fitted and then the ZFC curve was predicted with the obtained parameters. As occurred when ZFC data was initially fitted, the parameters that minimize residues in the FC fitting fail to reproduce the ZFC flat experimental response of the composite. In this case, T_B and diameters distributions were also obtained following the same procedure mentioned before and are presented in Fig. S4b and S4c. The T_B distribution highly deviate from the one presented in Fig. S3b. Also, the mean and median T_B were an order of magnitude bigger than the experimental ones.

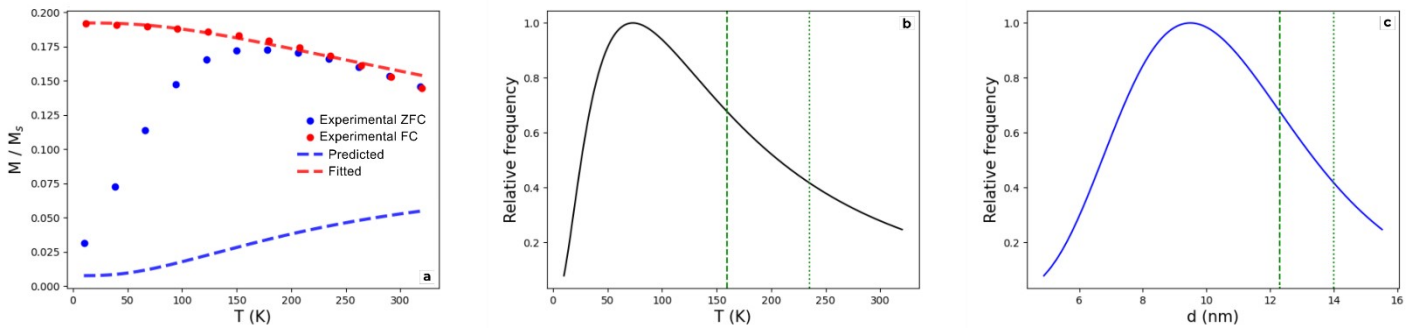


Figure S4. (a) ZFC and FC curves of PEDOT:DBS-Fe₃O₄ with $r_{EDOT,d} = 5$. Experimental data are represented with dots, and fitting and predicted data with short lines. (b) T_B distribution obtained from fitting for the PEDOT:DBS-Fe₃O₄ material prepared with $r_{EDOT,d} = 5$. (c) Diameter distribution obtained from fitting for PEDOT:DBS-Fe₃O₄ material prepared with $r_{EDOT,d} = 5$. Median and mean values are indicated by dashed and dotted lines, respectively.

Finally, in Fig. S5a the ZFC fitting and the FC prediction curves are presented for composite PEDOT:DBS-Fe₃O₄ obtained with $r_{EDOT,c} = 5$. Also, the T_B and diameter distributions are plotted in Fig. S5b and S5c. In similarity with the results founded for the dilute feed concentration case, it was not possible to obtain a single set of fitting parameters for both ZFC and FC curves.

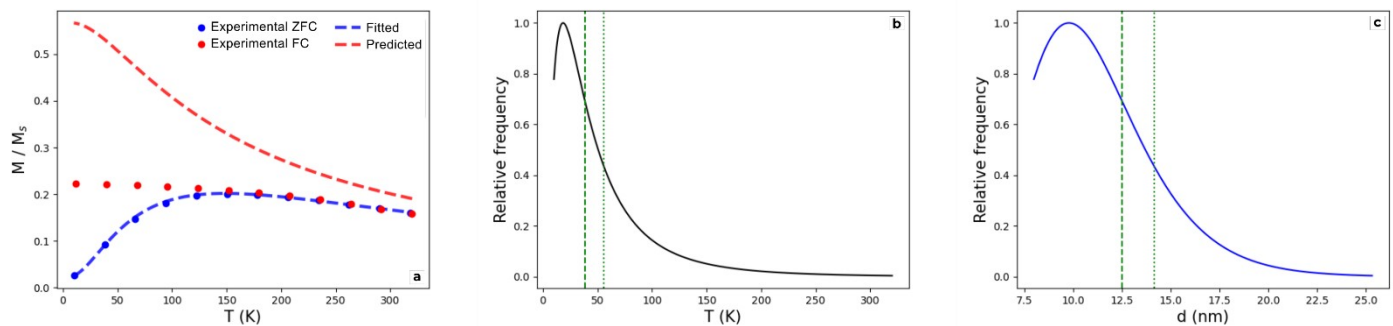


Figure S5. (a) ZFC and FC curves of PEDOT:DBS-Fe₃O₄ with $r_{EDOT,c} = 5$. Experimental data are represented with dots, and fitting and predicted data with short lines. (b) T_B distribution obtained from fitting for the PEDOT:DBS-Fe₃O₄ material prepared with $r_{EDOT,c} = 5$. (c) Diameter distribution obtained from fitting for PEDOT:DBS-Fe₃O₄ material prepared with $r_{EDOT,c} = 5$. Median and mean values are indicated by dashed and dotted lines, respectively.

Similar fitting results were obtained for composites with $r_{EDOT,d} = 2$ and $r_{EDOT,d} = r_{EDOT,c} = 10$.

To obtain a satisfactory fit for both ZFC and FC curves, we fit the experimental data by optimizing the temperature dependence of H in equations E2 and E3, respectively, following the framework described in ⁴. Instead of the applied field (H_{DC}), an effective field $H_{eff}(T) = H_{DC} + H_{int}$ is considered, where H_{int} is associated with the mean interactions present in the composite. The ferromagnetic coupling of MNP within a cluster lead us to define a correlation length L acting as an effective MNP diameter and determining a new effective blocking temperature $T_{B,eff} = K_{eff} V_{eff} / (25 k_B)$ as well as a normalized effective anisotropy constant $K_{eff} = K / \sqrt{N}$, where $V_{eff} = \pi L^3 / 6$ (assuming a spherical shape for the MNP) and N is the number of MNP per cluster.

As an example, in Fig. S6a we present the fits obtained for the ZFC and FC magnetization curves of $r_{EDOT,d} = 10$ measured with $H_{DC} = 8000$ A/m. Assuming the SEM determination of 50 particles per cluster and $M_s(T=0) = 15$ emu/g, the best fit was obtained for the temperature dependence of H_{eff} shown in Fig. S6b. The values $L = 17.3$ nm (mean), $s = 0.5$ (shape of the lognormal distribution) were determined imposing that H_{eff}^{ZFC} and H_{eff}^{FC} should be coincident for $T > T_B^{avg}$ and looking to reproduce the experimental distribution of T_B shown in Fig. 7b. The T_B and diameter distributions resulting from the ZFC and FC fit for the $r_{EDOT,c} = 10$ composite are plotted in Fig. S6c and S6d.

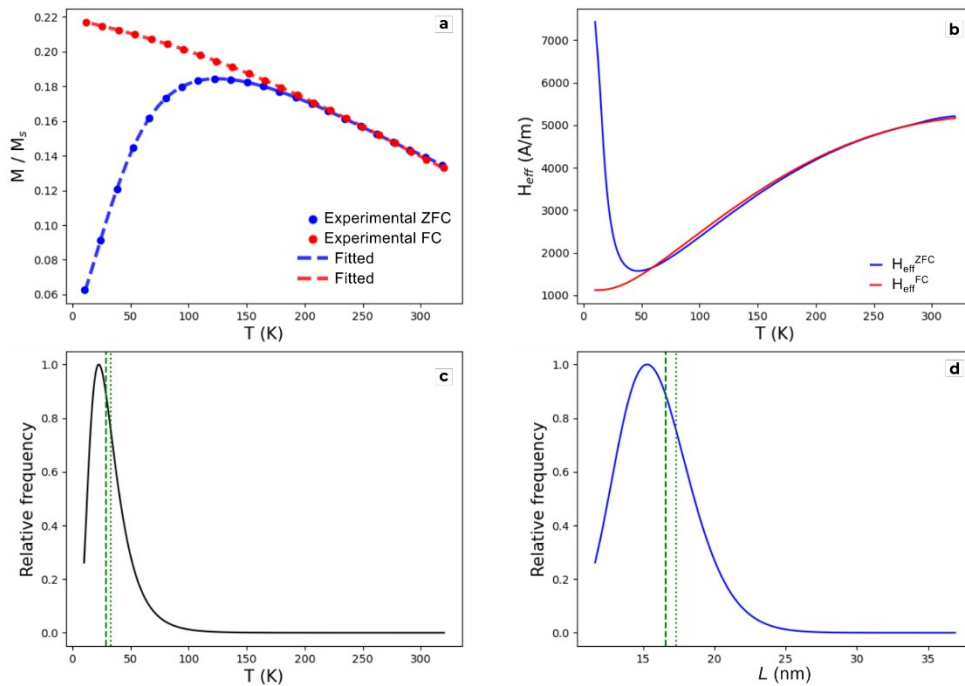


Figure S6. (a) ZFC and FC fits for ZFC and FC curves of PEDOT:DBS-Fe₃O₄ with $r_{EDOT,c} = 10$. Experimental data is represented with dots, and fitting data with short lines. (b) Optimized temperature dependence of H_{eff} used in the ZFC and FC fits presented in (a). (c) T_B distribution obtained from fitting for the PEDOT:DBS-Fe₃O₄ material prepared with $r_{EDOT,c} = 10$. (d) Effective MNP diameter distribution obtained from fitting for PEDOT:DBS-Fe₃O₄ material prepared with $r_{EDOT,c} = 10$. Median and mean values are indicated by a dashed and dotted lines, respectively.

The obtained H_{eff} ($H_{eff} < H_{DC}$) indicates a dipolar contribution as the main interaction between magnetic clusters with a temperature and history dependent demagnetization factor. We must point out the inconsistency obtained in the cluster's size L that, in order to be composed of $N = 50$ MNP, should have a value of the order of 30-50 nm.

References

- 1 G. Lavorato, M. Alzamora, C. Contreras, G. Burlandy, F. J. Litterst and E. Baggio-Saitovitch, *Part. Part. Syst. Charact.*, 2019, **36**, 1900061.
- 2 I. Muñoz Resta, G. Horwitz, M. Lanus Mendez Elizalde, G. A. Jorge, F. V. Molina and P. S. Antonel, *IEEE Trans. Magn.*, 2013, **49**, 4598–4601.
- 3 M. M. Lanús Mendez Elizalde, C. Acha, F. V. Molina and P. S. Antonel, *J. Phys. Chem. C*, 2020, **124**, 6884–6895.
- 4 F. Fabris, K.-H. Tu, C. A. Ross and W. C. Nunes, *J. Appl. Phys.*, 2019, **126**, 173905.
- 5 J. S. Micha, B. Dieny, J. R. Régnerd, J. F. Jacquot and J. Sort, *J. Magn. Magn. Mater.*, 2004, **272–276**, E967–E968.
- 6 H. Mamiya, M. Ohnuma, I. Nakatani and T. Furubayashim, *IEEE Trans. Magn.*, 2005, **41**, 3394–3396.

